ChemSusChem

Supporting Information

Light-Activated Superhydrophobicity of Sustainable Micro-Structured Spent Coffee Grounds-Based Interfaces via Fatty Acids Modulation

Seyed Shahrooz Zargarian,* Salvio Suárez-García, Javier Saiz-Poseu, Luca Zuppiroli, Massimiliano Lanzi, Daniel Ruiz-Molina, and Filippo Pierini*

Supporting Information

Light-activated Superhydrophobicity of Sustainable Micro-structured Spent Coffee Grounds-Based Interfaces via Fatty Acids Modulation

Seyed Shahrooz Zargarian[a*], Salvio Suárez-García[b], Javier Saiz-Poseu[b], Luca Zuppiroli[c], Massimiliano Lanzi[c], Daniel Ruiz-Molina[b], and Filippo Pierini[a*]

Seyed Shahrooz Zargarian (shzargar@ippt.pan.pl), Filippo Pierini (fpierini@ippt.pan.pl)

[a]Department of Biosystems and Soft Matter, Institute of Fundamental Technological Research, Polish Academy of Sciences, Pawińskiego 5B, Warsaw 02-106, Poland

Salvio Suárez-García (salvio.suarez@icn2.cat), Javier Saiz-Poseu (javier.saiz@icn2.cat), Daniel Ruiz-Molina (dani.ruiz@icn2.cat)

[b]Catalan Institute of Nanoscience and Nanotechnology (ICN2), CSIC and BIST, Campus UAB, Bellaterra, 08193 Barcelona, Spain

[c]Department of Industrial Chemistry "Toso Montanari", University of Bologna, Viale Risorgimento 4, 40136 Bologna, Italy

[*]Corresponding authors:

Seyed Shahrooz Zargarian (shzargar@ippt.pan.pl)

Filippo Pierini (fpierini@ippt.pan.pl)

Correspondence to: Filippo Pierini (fpierini@ippt.pan.pl)

Note 1:
The XRD peak observed at approximately 43° in both raw and annealed electrosprayed SCG (RSCG and HSCG) can be attributed to the inherent disordered carbon structures present within lignocellulosic materials, specifically those associated with lignin or lignin-based derivatives platforms.[1–4] The peak remained consistent across both treated and untreated samples, suggesting it is a fundamental characteristic of the SCG itself. Pyrolysis can lead to the intensification of this peak. During pyrolysis, the breakdown of the lignocellulosic matrix results in the formation of more carbon-rich structures. This process can enhance the degree of carbonization, thereby increasing the amount of disordered carbon, which in turn may intensify the peak at 43°.[5] The transformation during pyrolysis involves the degradation of lignin, cellulose, and hemicellulose, leading to a carbon structure that, while not perfectly ordered, shares characteristics with turbostratic carbon,[6] hence the observed peak enhancement. However, in this study, the mentioned peak did not intensify in HSCG, suggesting that the mild annealing process does not induce carbonization or drive the material toward a more graphitic or ordered structure.

Note 2:
90.2% of fatty acids remain in SCG after brewing.[7] The fatty acid content in SCG can vary due to several factors, including the extraction method, the type of solvent used, temperature, and the particle size of the SCG. The literature reports oil yields ranging from 6% to 21.5%, with hexane being the most common solvent employed.[7] The fatty acid composition in SCG is predominantly linoleic acid (44–50%) and palmitic acid (35–40%), with smaller quantities of stearic (7–8%) and oleic (7–8%) acids. The composition of these fatty acids in SCG is also significantly influenced by the origin of the coffee beans. Since our SCG was sourced from Costa Coffee, our SCG samples consisted mainly of spent grounds of a blend of Arabica and Robusta beans.[8,9] Existing literature on similar blends supports these findings. For instance, Kondamudi et al. reported a 13.4% fatty acid content in Arabica-Robusta SCG using hexane extraction, with palmitic acid at 51.4%, linoleic at 40.3%, and stearic at 8.3%.[10] Another study examined SCG's oil from 12 coffee brands, all Arabica-Robusta blends via Soxhlet extraction, finding linoleic acid at 43.2%, palmitic at 31.8%, oleic at 12.7%, stearic at 7.3%, and arachidic at 3.0%.[11] Additionally, Cruz et al. analyzed 50 SCG samples from 14 coffee brands using Soxhlet extraction with petroleum ether, identifying linoleic acid at 44.2%, palmitic at 32.8%, oleic at 10.3%, and stearic acid among others.[12]

Table S1: Melting temperatures and thermal degradation onset temperatures of the primary fatty acids in SCG alongside its major biopolymeric components

SCG's Compositional Components	Melting Temperature (°C)	Thermal Degradation Onset Temperature (°C)	Reference
Linoleic acid	-12	229 (boiling point)	CRC Handbook of Chemistry and Physics
Palmitic acid	62.9	175	[13]
Oleic acid	14	180	[14]
Cellulose	-	260	[15]
Hemicellulose	-	220	[16]

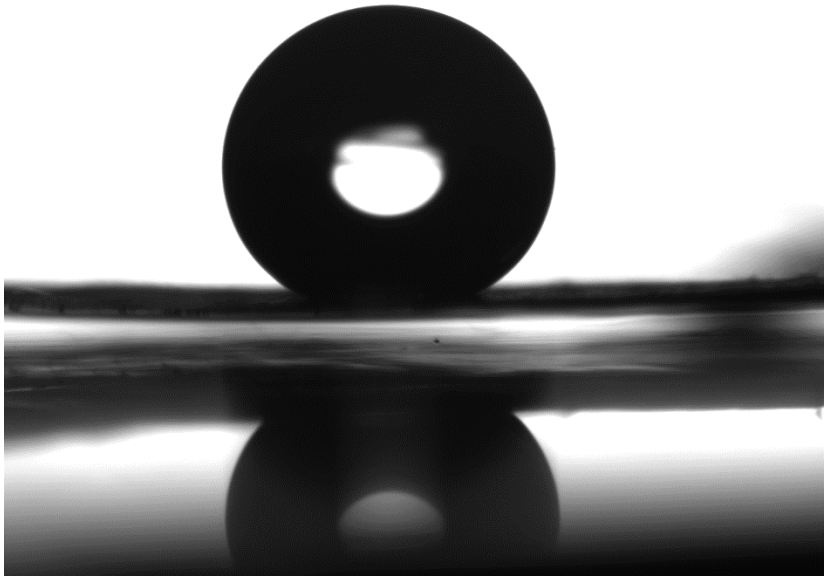

Sup. Fig. 1: A water droplet on the HSCG surface. The contact angle is 152°, demonstrating the surface's excellent water repellence.

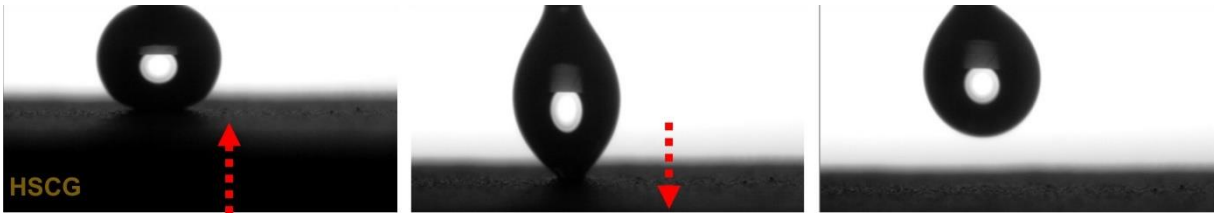

Sup. Fig. 2. Interaction between the HSCG surface and a water droplet during contact angle measurement. The sequence shows the HSCG coating surface approaching the water droplet, making contact, and then retracting, with the droplet remaining intact on the needle tip.

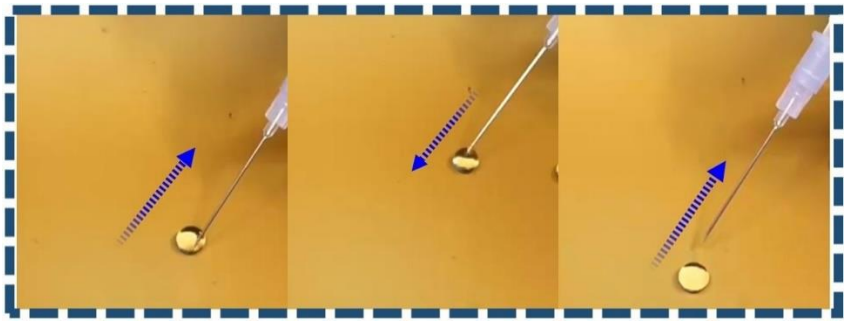

Sup. Fig. 3. Manipulation of a water droplet on the HSCG surface using a needle tip. The water droplet can be easily guided across the superhydrophobic surface, indicating the low adhesion and high mobility characteristic of the HSCG coating.

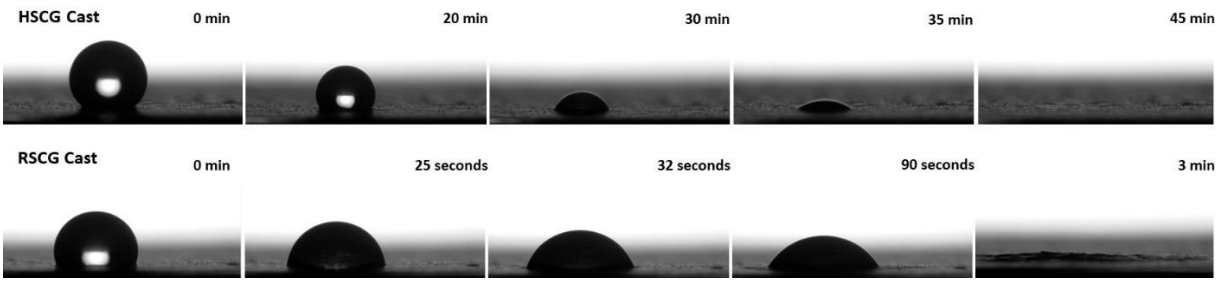

Sup. Fig. 4. Hydrophobic behavior of RSCG and HSCG cast. While the HSCG cast sample exhibits some degree of hydrophobicity, it allows water to wet the surface after approximately 20 minutes, and maneuvering a water droplet across its surface is not feasible.

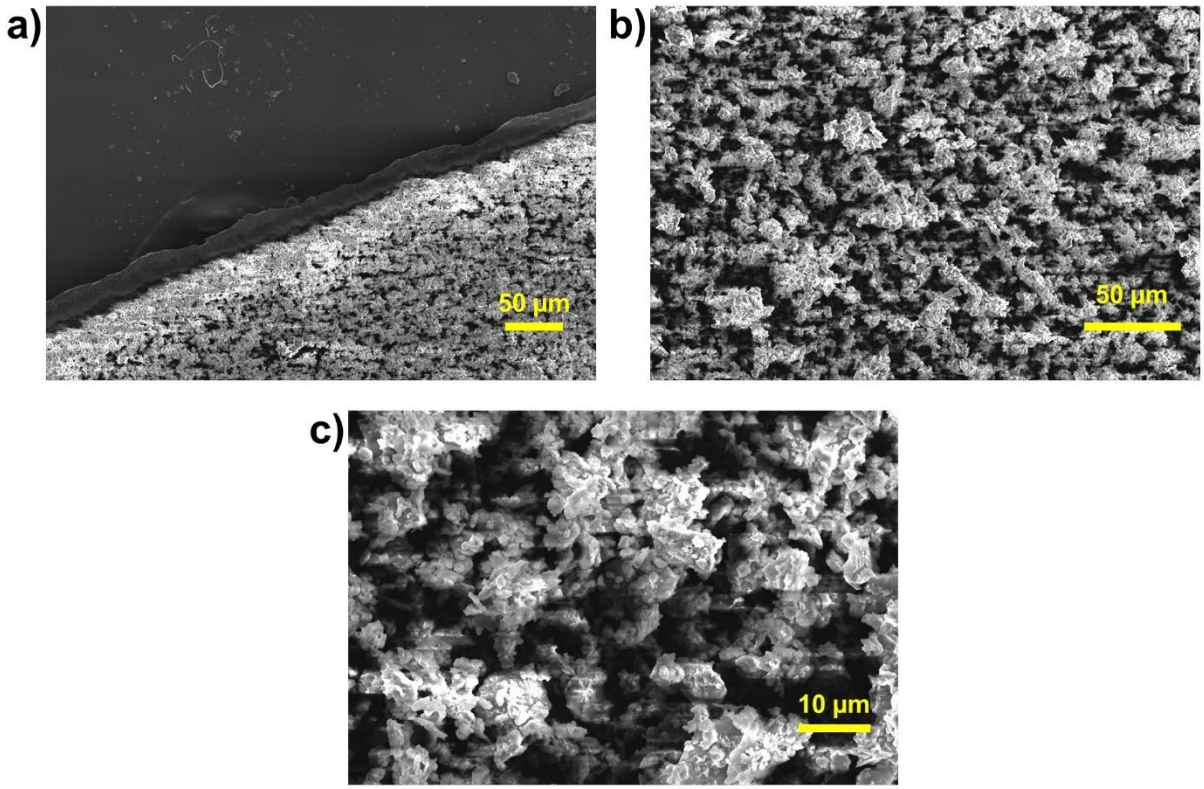

Sup. Fig. 5. Initial SEM imaging attempt of the electrosprayed SCG coating. The images show significant surface charging. a) coating edge, b) low magnification, and c) high magnification of RSCG coating.

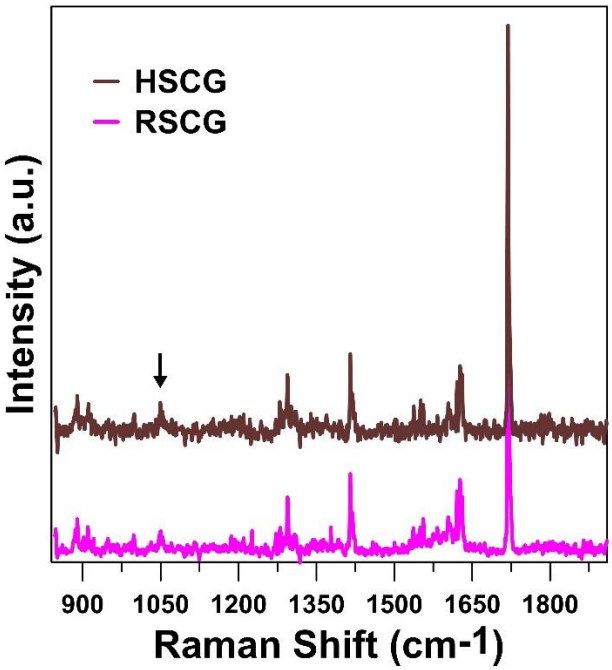

Sup. Fig. 6. Raman spectra of RSCG and HSCG. Both spectra exhibit similar features. A slight increase in the intensity of the 1050 cm^{-1} peak in HSCG may suggest a higher surface presence of fatty acids after annealing.

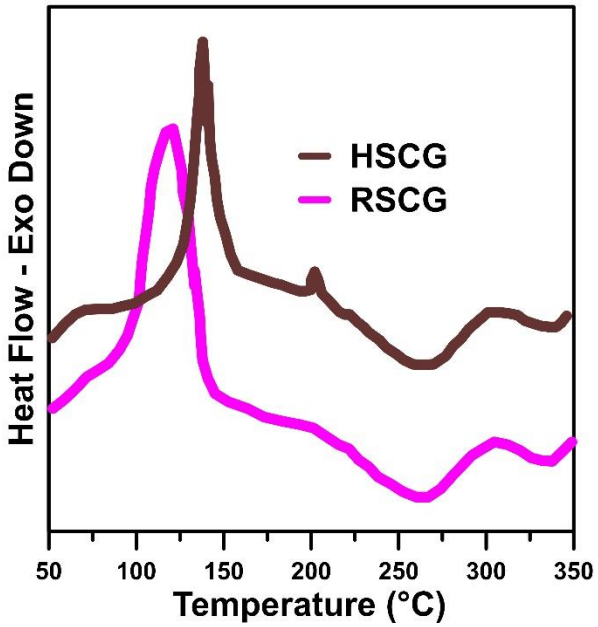

Sup. Fig. 7. DSC thermograms of RSCG and HSCG, highlighting the effects of mild annealing on thermal transitions. The results reveal a notable shift in the endothermic peak from RSCG (ranging from 70–140 °C with an enthalpy of 58.08 J/g) to a sharper and narrower peak in HSCG (110–155 °C, 49.33 J/g). This transformation suggests a decrease in moisture content in HSCG due to the annealing process. Conversely, the exothermic degradation behavior, observed between 200–320 °C with an approximate enthalpy of 6.5 J/g, remains consistent between the two samples.

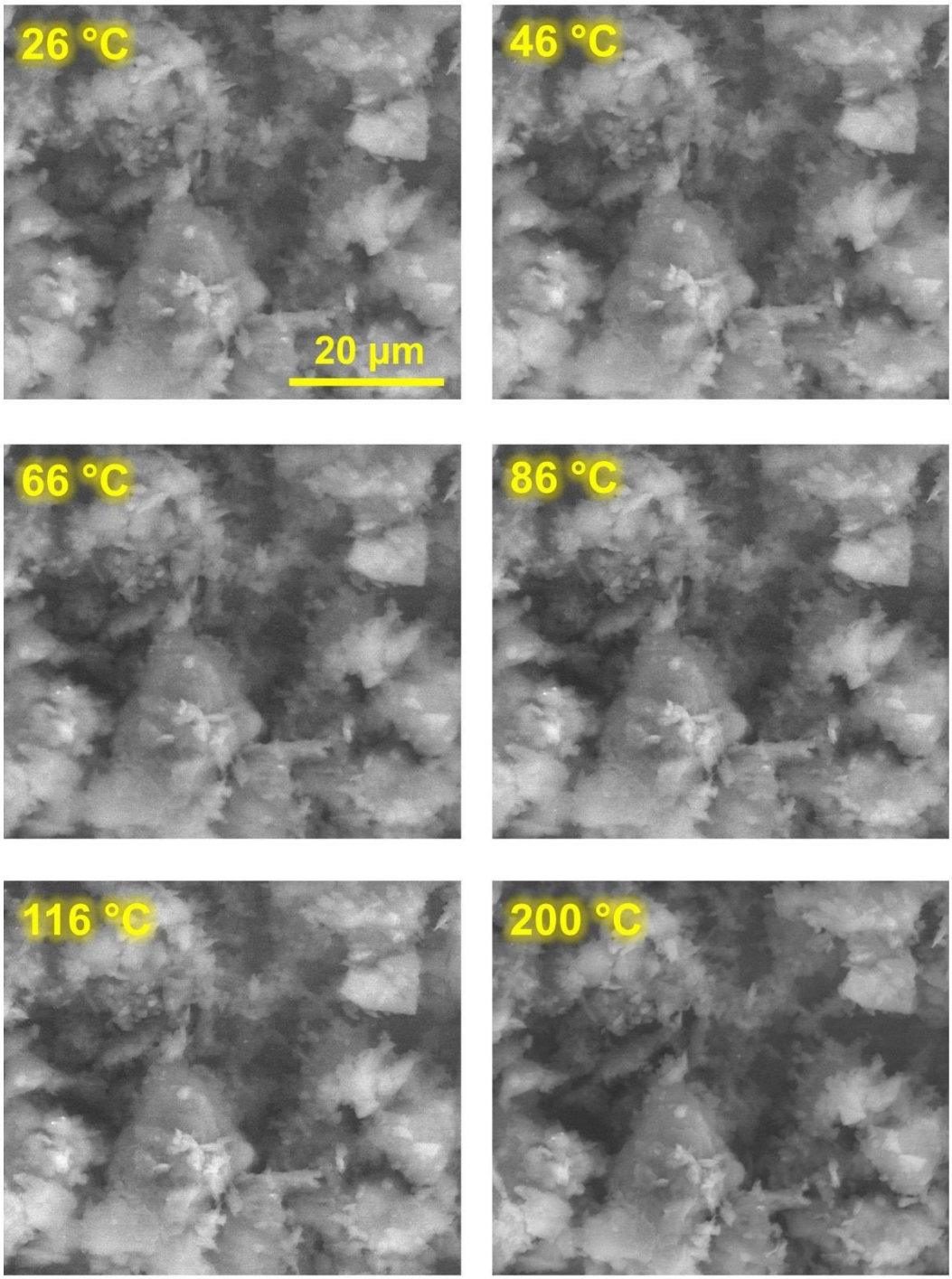

Sup. Fig. 8. Imaging of RSCG conducted with an SEM device equipped with a temperature ramping capability. The images reveal no changes in surface morphology during the heating process up to 200°C, indicating that the superhydrophobic behavior of HSCG is not due to morphological alterations.

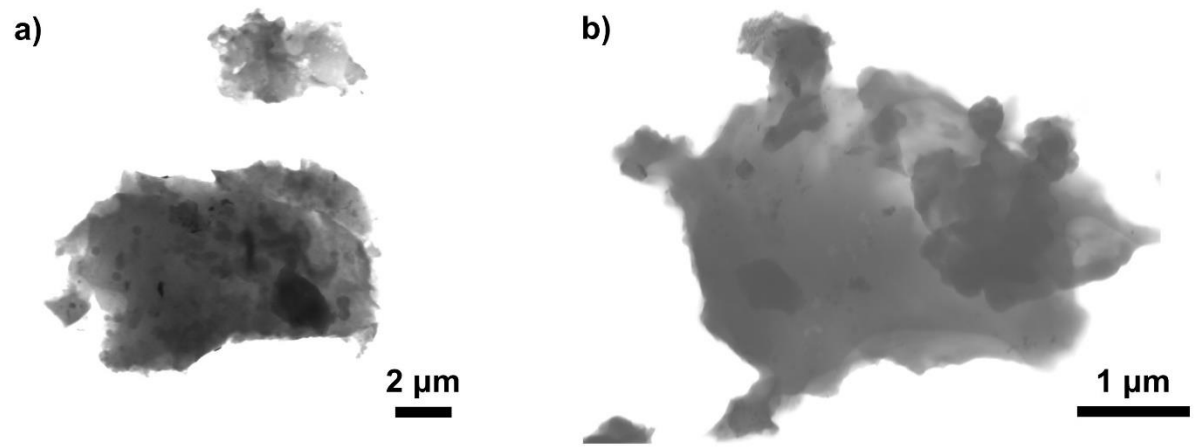

Sup. Fig. 9. STEM images and EDX analysis of SCG samples: (a) RSCG and (b) HSCG. Quantitative EDX analysis indicated C and O percentages of 87.4% and 11.65% for RSCG and 86.4% and 13.2% for HSCG. The results show no detectable morphological changes, and the compositional changes post-annealing are consistent with XPS findings.

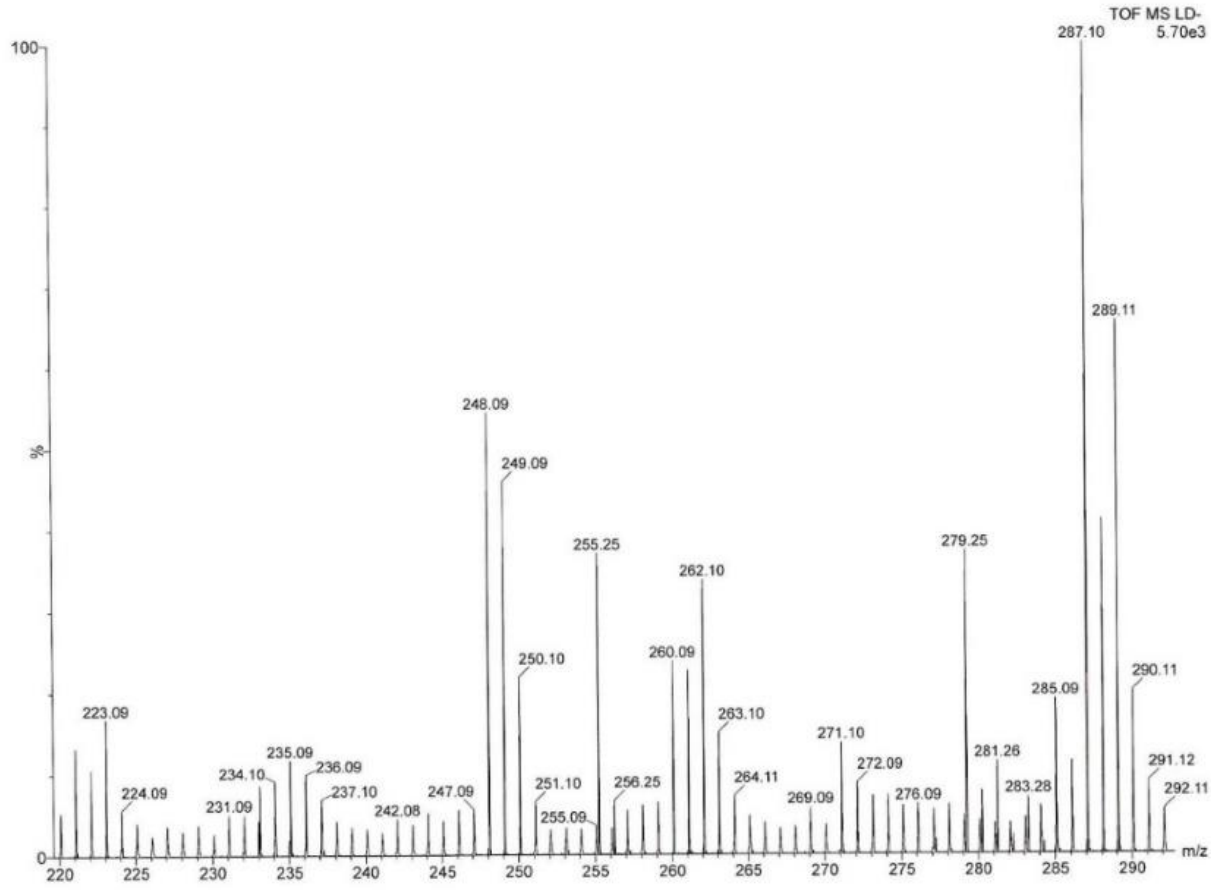

Sup. Fig. 10. MALDI-TOF MS spectrum of SCG extract in negative ion mode, showing prominent peaks corresponding to deprotonated fatty acids: palmitic acid (m/z 255), linoleic acid (m/z 279), and oleic acid (m/z 281). These results confirm the presence of major SCG fatty acids, as reported in the literature.

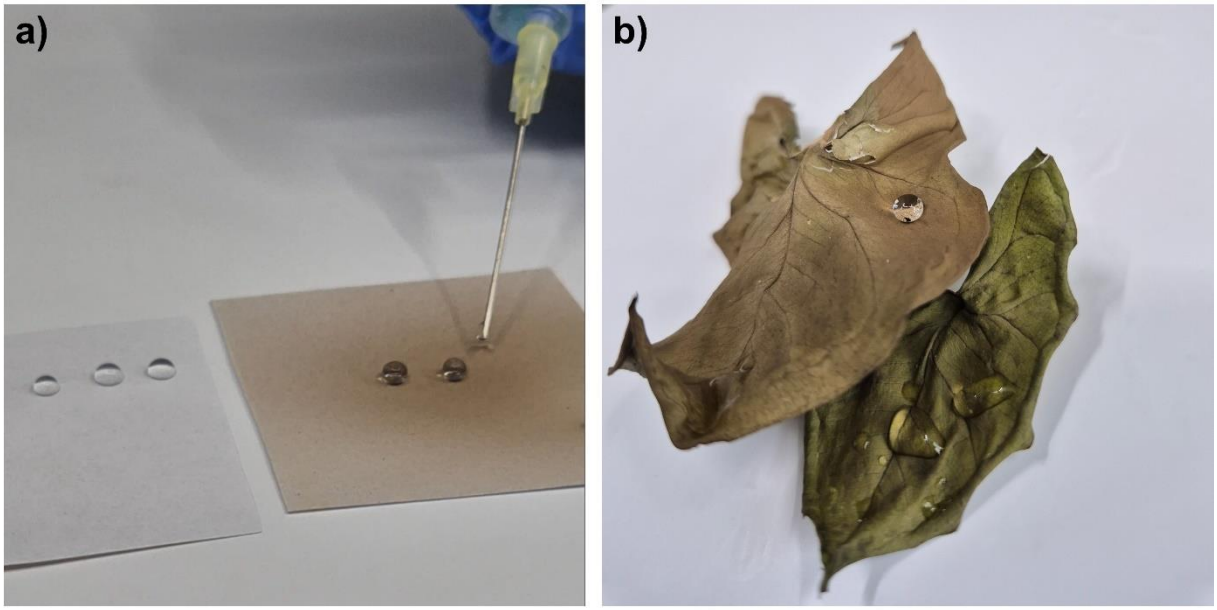

Sup. Fig. 11. Demonstration of the ease of electrospraying SCG microparticles onto various surfaces and their transformation into a superhydrophobic state. a) Camera photo showing two pieces of paper, one electrosprayed with SCG microparticles, which exhibits superhydrophobic behavior with water droplets beading on its surface, while the untreated paper remains hydrophilic, b) illustrating the same effect on a plant leaf.

Supplementary Video 1. Superoleophilicity of the HSCG coating. A drop of olive oil is placed on the HSCG, which instantly wets the surface.

Supplementary Video 2. Water droplets rolling off from the HSCG surface

Supplementary Video 3. Guiding the water droplets on the HSCG surface using a needle tip.

Supplementary Video 4. Demonstration of the self-cleaning properties of the HSCG superhydrophobic surface. At the end of the video, accumulated dirt is effortlessly removed with a napkin.

References

(1) Gea, S.; Siregar, A. H.; Zaidar, E.; Harahap, M.; Indrawan, D. P.; Perangin-Angin, Y. A. Isolation and Characterisation of Cellulose Nanofibre and Lignin from Oil Palm Empty Fruit Bunches. *Materials (Basel)* **2020**, *13*.

(2) Zhang, J.; Zhao, X.; Kong, Q.; Wang, X.; Lou, T. Preparation of chitosan/DADMAC/lignin terpolymer and its application of dye wastewater flocculation. *Polym. Bull.* **2022**, *79*, 7479–7490.

(3) Gomide, R. A. C.; de Oliveira, A. C. S.; Rodrigues, D. A. C.; de Oliveira, C. R.; de Assis, O. B. G.; Dias, M. V.; Borges, S. V. Development and characterization of lignin microparticles for physical and antioxidant enhancement of biodegradable polymers. *J. Polym. Environ.* **2020**, *28*, 1326–1334.

(4) Ye, X.-X.; Luo, W.; Lin, L.; Zhang, Y.; Liu, M. Quaternized lignin-based dye dispersant: Characterization and performance research. *J Dispers Sci Technol* **2017**, *38*, 852–859.

(5) Mukherjee, A.; Borugadda, V. B.; Dynes, J. J.; Niu, C.; Dalai, A. K. Carbon dioxide capture from flue gas in biochar produced from spent coffee grounds: Effect of surface chemistry and porous structure. *Journal of Environmental Chemical Engineering* **2021**, *9*, 106049.

(6) Petrenko, I.; Summers, A. P.; Simon, P.; Żółtowska-Aksamitowska, S.; Motylenko, M.; Schimpf, C.; Rafaja, D.; Roth, F.; Kummer, K.; Brendler, E.; *et al.* Extreme biomimetics: Preservation of molecular detail in centimeter-scale samples of biological meshes laid down by sponges. *Sci. Adv.* **2019**, *5*, eaax2805.

(7) Atabani, A. E.; Al-Muhtaseb, A. H.; Kumar, G.; Saratale, G. D.; Aslam, M.; Khan, H. A.; Said, Z.; Mahmoud, E. Valorization of spent coffee grounds into biofuels and value-added products: Pathway towards integrated bio-refinery. *Fuel* **2019**, *254*, 115640.

(8) Klikarová, J.; Řeháková, B.; Česlová, L. *Evaluation of regular and decaffeinated (un)roasted coffee beans based on antioxidant capacity and total phenolic content*; University of Pardubice, 2023.

(9) Ludwig, I. A.; Mena, P.; Calani, L.; Cid, C.; Del Rio, D.; Lean, M. E. J.; Crozier, A. Variations in caffeine and chlorogenic acid contents of coffees: what are we drinking? *Food Funct* **2014**, *5*, 1718–1726.

(10) Kondamudi, N.; Mohapatra, S. K.; Misra, M. Spent coffee grounds as a versatile source of green energy. *J. Agric. Food Chem.* **2008**, *56*, 11757–11760.

(11) Bijla, L.; Ibourki, M.; Bouzid, H. A.; Sakar, E. H.; Aissa, R.; Laknifli, A.; Gharby, S. Proximate composition, antioxidant activity, mineral and lipid profiling of spent coffee grounds collected in morocco reveal a great potential of valorization. *Waste Biomass Valor.* **2022**, *13*, 4495–4510.

(12) Cruz, R.; Cardoso, M. M.; Fernandes, L.; Oliveira, M.; Mendes, E.; Baptista, P.; Morais, S.; Casal, S. Espresso coffee residues: a valuable source of unextracted compounds. *J. Agric. Food Chem.* **2012**, *60*, 7777–7784.

(13) Chen, H.; Wang, Y.; Cao, P.; Liu, Y. Effect of temperature on thermal oxidation of palmitic acid studied by combination of EPR spin trapping technique and SPME-GC-MS/MS. *Food Chem.* **2017**, *234*, 439–444.

(14) García-Zapateiro, L. A.; Franco, J. M.; Valencia, C.; Delgado, M. A.; Gallegos, C. Viscous, thermal and tribological characterization of oleic and ricinoleic acids-derived estolides and their blends with vegetable oils. *Journal of Industrial and Engineering Chemistry* **2013**, *19*, 1289–1298.

(15) CDC - NIOSH Pocket Guide to Chemical Hazards - Cellulose https://www.cdc.gov/niosh/npg/npgd0110.html (accessed Feb 2, 2025).

(16) Yang, H.; Yan, R.; Chen, H.; Lee, D. H.; Zheng, C. Characteristics of hemicellulose, cellulose and lignin pyrolysis. *Fuel* **2007**, *86*, 1781–1788.